VTT Technical Research Centre of Finland

Scale effects on tip loaded propeller performance using a RANSE solver

Sánchez-Caja, Antonio; González-Adalid, J.; Pérez-Sobrino, M.; Sipilä, Tuomas

Link to publication

Scale Effects on Tip Loaded Propeller Performance Using a RANSE Solver

A. Sánchez-Caja[a], J. González-Adalid[b], M. Pérez-Sobrino[b] and T.Sipilä[a]

[a]VTT-Technical Research Center of Finland,
[b]SISTEMAR,

ABSTRACT

Traditionally, the quality of alternative propeller designs at full scale has been assessed by means of model scale tests. Due the large differences in Reynolds numbers between model and full scales, model-scale-based performance predictions may be questionable in cases where viscous effects are dominant. This paper presents a numerical study about scale effects on performance coefficients for a CLT propeller with different endplate geometries. Twelve endplate shape variations were analyzed in model and full scale using RANS code FINFLO. The SST k-ω turbulence model is used as basic model for the study. Additional computations are made with other turbulence models. A special procedure for the generation of the computational grids is implemented to minimize computational errors in the comparison of the alternative geometries. The study provides also a RANS-based scale effect on the shape of radial circulation distribution predicted for different geometry variations. The research work gives an insight into which type of modifications at full scale could be analyzed by model scale viscous flow theory or model tests in ranking alternative designs. Differences found between model and full scale numerical results make model scale analysis questionable for some specific type of modifications when full-scale performance is sought.

Keywords: scale effects, tip loaded propeller, CLT, RANS, extrapolation, circulation,

1. INTRODUCTION

Model tests have usually been used to predict the performance of marine propellers in full scale. Deficiencies in predictions of propeller performance and/or cavitation behavior for especial types of propellers have been sometimes noticed in particular applications like high skewed propellers, ducted propellers and tip loaded propellers. Such deficiencies have led the 27th ITTC (International Towing Tank Conference) to recommend examining the scaling procedures and to encourage establishing research programs intended to clarify scaling problems.

From the CFD standpoint, limitations of potential-flow-based methods to predict scale effects have led researchers to focus on RANS approaches. Scale effects on general propellers have been computed for open propellers in Stanier (1998), Funeno (2002), Li et al. (2006) and Koushan and Krasilnikov (2008). For ducted propellers, scale effects have been investigated in Abdel-Maksoud and Heinke (2002), Krasilnikov et al (2007) and Mertes and Heinke (2008). Scale effects on podded propellers are presented in Chicherin et al (2004), Lobachev and Chitcherin (2001) and Sanchez-Caja et al. (2003). Effort to reach a deeper understanding on how turbulence models behave for the prediction of scale effects on propellers has been made recently. Krasilnikov, et al. (2009) has studied the influence of blade skew, loading and area ratio on scaling using the FLUENT solver with the SST k-ω model. Müller et al., (2009) used the ANSYS-CFX solver with the SST turbulence model to numerically analyze a variety of propellers at model and full scale in open water. Kawamura and Omori (2009) presented a computational study on propeller scaling of open water performance for 5-bladed and 4-bladed propellers using FLUENT and the SST k-ω model with its high and low Reynolds number version. He found that scale effects exist in both pressure and frictional forces. Both forces affect the scale effect in thrust, while the frictional force contributes mainly to the scale effect in torque. Limitations on turbulence modeling for simulating propeller flow have been reported in Li et al.

Corresponding author: Antonio Sánchez-Caja, Ship Hydrodynamics, VTT Technical Research Centre of Finland, Tietotie 1 A, PL 1000 02044 VTT Espoo, Finland. Tel.: +358 50 352 4743; Fax: +358 20 722 7075; E-mail: antonio.sanchez@vtt.fi

(2006) and the need for a good grid quality has been stressed from the standpoint of wall treatment within the turbulence model.

Generally, model scale predictions are more challenging than full scale ones due to the possible simultaneous presence of different flow regimes and the difficulty to accurately predict transition in the computations. Separation may exist at model scale, which is not present at full scale. Efforts to improve transition models from laminar to turbulent flow have been made recently in Menter et al. (2006).

Historically, RANS computations on CLT propellers were made within EU project Leading Edge and reported in Sánchez-Caja et al. (2006). Comparison of scale effect on flow features like tip vortices at model and full scale was presented. Hsin et al. (2010) and Cheng et al. (2010) studied tip-loaded propellers of CLT and Kappel type. They used both a panel method and a RANS solver in the analysis. Scale effects were found for both propeller types larger than for conventional propellers. In addition, scale effects were studied in Haimov et al. (2011) for CLT propellers and difficulty to obtain grid-independent results using unstructured meshes was illustrated. Gaggero & Brizzolara (2011) have analyzed a CLT propeller using the RANS code StarCCM+ and a panel code. They presented numerical analysis under cavitation conditions and comparison with experiments in Bertetta et al. (2012), being the main focus comparison of panel method and RANS results also from the standpoint of scaling. They presented radial distributions of circulation obtained with the panel code.

Recently, systematic variations of the endplate geometry for end-plate propellers were made using RANS code FINFLO in order to assess the impact of the blade tip shape on propeller performance at full scale. Some results were anticipated in Sánchez-Caja, et al. (2012) and the final analysis was reported in Sánchez-Caja, et al. (2014). In the present paper, the same geometry variations will be analyzed from the standpoint of scaling effects. Scale effects will be computed using mainly the SST k-ω turbulence model even though Chien's k-ε and Spalart Allmaras turbulence models will be also used for a reference geometry. A special procedure for the generation of the computational grids is implemented in order to minimize computational errors in the comparison of the alternative geometries. In this study, we focus on non-cavitating flow conditions in order to assess the pure impact of the plate shape on scaling, leaving for future work the scaling of cavitating flows. The work presents radial distributions of circulation obtained with the RANS solver, which is a novelty for this type of propellers since previous researchers have focused more on circulations based on potential flow analysis. The analysis allows evaluating the scale effect on the shape of the circulation curve.

This work has been made within the EU Project TRIPOD where CLT propellers were studied from the standpoint of efficiency improvement.

2. NUMERICAL METHOD

The RANS equations are solved using the FINFLO code initially developed at the Laboratory of Aerodynamics at Helsinki University of Technology (Siikonen et al., 1990). A description of the numerical method including discretization of the governing equations, solution algorithm, etc. can be found also in Sanchez-Caja et al. (1999). The code employed initially the artificial compressibility method to solve the RANS equations and has been recently extended to incorporate the pressure correction method. The momentum equations can be written in the following form

$$\rho \frac{D\vec{V}}{Dt} + \nabla p - \mu \nabla^2 \vec{V} = \rho \vec{g} + \vec{F}_{BF} \qquad (1)$$

where $\vec{V}$ is the velocity vector, ρ is the density, μ is the dynamic viscosity, $\vec{g}$ the acceleration of gravity and $\vec{F}_{BF}$ are possible body forces. The equation can be expressed in terms of a vector U of conservative variables $(\rho, \rho u, \rho v, \rho w, \rho k, \rho \varepsilon)^T$, where u, v and w are the absolute velocity components; k is the turbulent kinetic energy and ε is the dissipation of k. For the steady-state analysis with a full representation of the propeller, the equations are solved in a co-ordinate system that rotates around the x-axis with an angular velocity Ω. In that case, the RHS of the momentum equation has the additional component $(0, 0, \rho\Omega w, -\rho\Omega v, 0, 0)$. For time-accurate simulations, the source terms for the turbulence equations are retained, but there are no source terms in the momentum equations except gravitation.

FINFLO solves the RANS equations by a finite volume method using either the density-based pseudo-compressibility method or the pressure correction method. The computations presented in this paper have been made with the pressure correction method (Siikonen, 2011).

In FINFLO, the solution is extended to the wall. An essential feature in the code is to separate flux calculation from the solution. Then the code may use either Roe's flux-difference splitting for compressible or an upwind based scheme for incompressible flows. A multigrid method may be used for the acceleration of convergence even though with the pressure-based solution this kind of multigrid acceleration is still rare (Siikonen, 2011). Solutions in coarse

grid levels are used as a starting point for the calculation in order to accelerate convergence. Chien's low Reynolds number k-ε model was used in the computations.

The boundary conditions for the cases studied are set as usual. The propeller blades are modeled as rotating non-slip surfaces with the velocity field matching the propeller rotational speed. A uniform flow condition is applied to the inlet and peripheral surfaces. At the outlet, the streamwise gradients of the flow variables as well as the pressure difference are set to zero. For the uniform flow computations, only the portion between two contiguous blades has been used due to the periodicity of the solution.

3. GEOMETRY VARIATIONS

A four-bladed controllable pitch propeller working under a moderately unloaded off-design condition has been chosen as reference geometry for the study. The choice of the operational point was related to a previous optimization study (Sánchez-Caja, et al., 2014) in a challenging condition for CLT propellers since they are expected to be more beneficial at high loads. In such condition, scale effects on efficiency are expected to be larger than at the design point. The propeller is a 4.38 meter diameter with a pitch diameter ratio of 1.1. The hub diameter ratio is 0.33. The expanded area ratio is 0.52 and the skew is moderate. The endplate is located to the pressure side of the blade. The onset flow for the calculations corresponds to an advance coefficient of 0.90. Full and model scale performances are studied. The scale factor is 17.962, which corresponds to a Reynolds number at model scale of 10^6 and at full scale of $5*10^7$.

Several types of endplate modifications were analyzed using the SST k-ω and Chien's low Reynolds number k-ε turbulence models. They include variations in plate contraction angle, plate sweep, flap angle and plate cutting.

Table I shows the cross relation among the variations of geometry for twelve cases analyzed for the 4-bladed propeller relative to the baseline. An integer number representative of the strength of the modification is presented in each column. The larger the number, the stronger the modification and vice versa. Index number 0 means value of the baseline propeller.

Table I. Cross relation among the variations of geometry for twelve cases analyzed for the 4-bladed propeller. 0= baseline; negative number, negative modification; positive number, positive modification relative to baseline

No	contract	flap	sweep	cutting
1	0	0	0	0
2	0	1	0	0
3	0	2	0	0
4	-1	0	0	0
5	1	0	0	0
6	2	0	0	0
7	3	0	0	0
8	0	0	-1	0
9	0	0	1	0
10	0	0	0	1
11	0	0	0	2
12	0	0	0	3

3.1 Plate Contraction

The contraction angle of the plate was defined as a function of the trailing edge (TE) length and four variations were studied (Fig. 1). With the grid generation code, the length of the TE line of the propeller was changed and this was the parameter used for defining the radial inclination of the plate. Maximum inclination (contraction) is represented by the shortest TE length, which is labeled as the 99 %, and minimum inclination by the longest TE length, labeled as 106 % in the sketch. In other words, the inclination varies inversely proportional to the TE length. The 100 % represents initial location of the plate corresponding to an estimation of the endplate aligned with the flow at other working condition (the design point). The TE lengths were 99, 102, 104 and 106 percent. As shown in Table I, contraction variations were labeled with numbers 4, 5, 6 and 7.
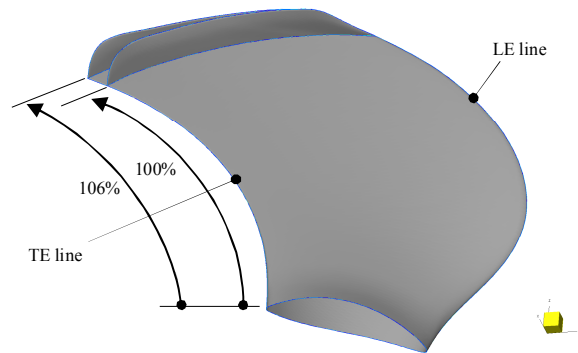
Figure 1. Sketch for the definition of plate contraction

3.2 Flap angle

By "flap angle", we mean the angle of the plate relative to an axis passing through the chord line at the juncture of the blade and endplate (Fig. 2). Zero angle means 'plate at ordinary position', i.e. a position such that the plate sections made with planes containing the propeller axis are parallel to the axis (baseline propeller). The angle is positive for the endplate outer edge rotated inwards, towards the hub. Negative angles (outward rotation) were not considered as they result in an increase of the propeller diameter, which would change the basic criterion for comparison (a given diameter). Three flap angles were studied: 0, 10 and 30 deg. As shown in Table I, flap angle variations were labeled with numbers 1, 2 and 3.
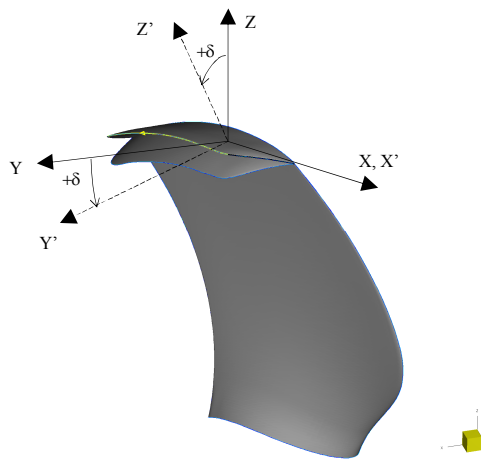

Figure 2. Sketch for the definition of flap angle (δ)

3.3 Plate sweep

If we consider the plate as half a wing with very low aspect ratio, modifications that resemble forward or backward swept wings may be introduced in the endplates (Fig. 3) by moving the outer edge of the endplate forward or backward. Sweep variations were labeled with numbers 8 (back sweep) and 9 (forward sweep), see Table I.
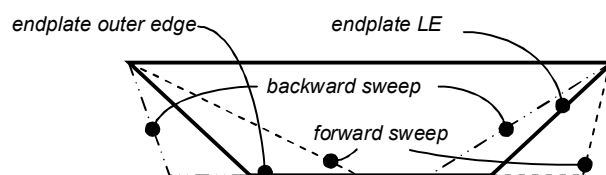

Figure 3. Sketch for the definition of sweep

3.4 Plate cutting

The last type of modification was plate cutting (Fig. 4). Three cuts were made. The largest cut reached the endplate border at a location close to mid-chord of the endplate root. The modifications did not affect the leading edge (LE). As shown in Table I, cuttings were labeled with numbers 10 (large), 11 (medium) and 12 (small).
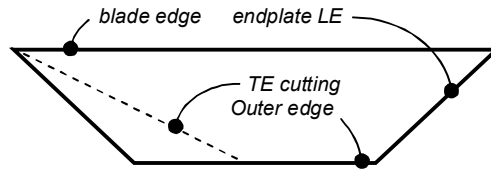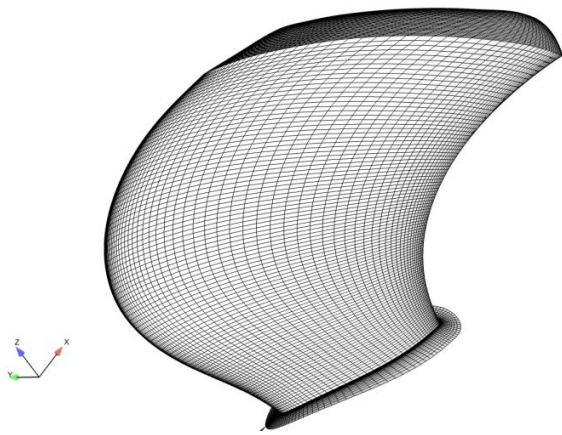

Figure 4. Sketch for the definition of plate cutting

Figure 5. Grid on the suction side of the propeller blade. Endplate located on the pressure side.
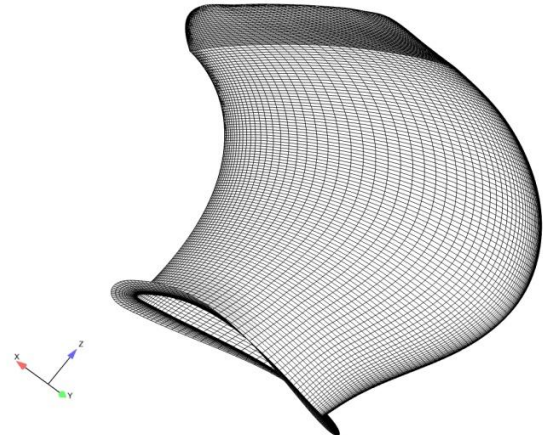

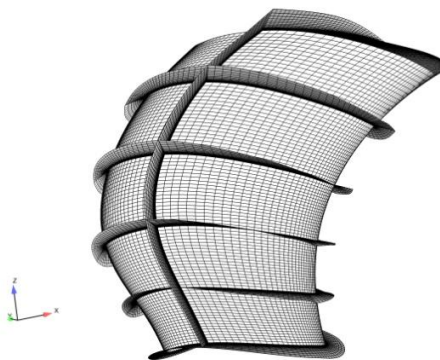*Figure 6. Grid on the pressure side of the propeller blade.*

Figure 7. Grid cuts at constant indexes in the block surrounding the blade.

4. MESH GENERATION

We have tried to reduce relative numerical errors between grids by performing geometrically similar structured grids. For automating the grid generation process, we use an in-house developed program run with the help of templates. By using the same templates for the different endplate shapes, we guaranty the same number and distribution of cells for the various meshes as well as a similar topology. In this way, numerical errors in the comparison of performances for different endplate shapes are reduced.

An O-O topology was used around the blades and endplates with the aim of reducing the number of cells for a given accuracy. This allowed achieving a good control of the grid orthogonality over the propeller surfaces. Figures 5 and 6 show the distribution of cells on the blade surfaces on the suction and pressure sides of the blade, respectively. Figure 7 shows constant index cuts of the mesh on the direction normal to the blade.

A number of 128 cells around the blade in the chordwise direction and 96 in the radial direction were used, respectively. The full scale grids had 16 more cells in the direction normal to the blade surface. The cell size was adjusted especially at the leading, trailing and endplate edges in the regions of high curvature. The mesh consisted of 19 blocks per blade. The numbers of cells per block in each of the three index directions were multiple numbers of 16 in order to apply techniques of multigrid acceleration. The size of the fine grid was about 2.1 million cells per blade in the model scale and 2.4 in full scale. Cyclic boundary conditions were used for the calculations in uniform flow in order to model the space between blades, avoiding unnecessary large grids.

5. CONVERGENCE

An uncertainty study was initially made. Three meshes were built for a reference propeller with cell ratios of 1, 2 and square root of 2 (coarse, fine and medium grid). The coarse mesh is obtained by removing every other grid point in the three grid index directions from the fine one. Tables II, and III show the performance coefficients expressed as percentages of the fine grid solutions in terms of thrust, torque and efficiency for the coarse, medium and fine grid, respectively. They correspond to computations made with the SST k-ω in full scale and model scale, respectively. Tables IV and V illustrate the variation on performance coefficients for the Chien's k-ε model in full and model scale. It is apparent that the efficiencies in Table V for the coarse and medium grid are not as close to the fine grid as in the other Tables. As will be shown in the next section, this is due to the prediction of laminar flow detachment at model scale with the k-ε model in a significant portion of the blade near the hub, which requires higher resolution and presents higher uncertainty than undetached flow.

As the fine grid solution uses the coarse grid one as a starting point, the results for the fine and coarse grid are computed for all the alternative shapes tested.

The computations were performed on Windows environment with Intel® Xeon® 2.67GHz processors.

Table II. Performance coefficients expressed as percentages of the fine grid solutions for the coarse, medium and fine grids. SST k-ω turbulence model in full scale

	K_T	K_Q	η
coarse	101.53	101.73	99.80
medium	99.85	100.25	99.60
fine	100.00	100.00	100.00

Table III. Performance coefficients expressed as percentages of the fine grid solutions for the coarse, medium and fine grids. SST k-ω turbulence model in model scale

	K_T	K_Q	η
coarse	102.33	102.55	99.782
medium	100.68	100.82	99.862
fine	100.00	100.00	100.00

Table IV. Performance coefficients expressed as percentages of the fine grid solutions for the coarse, medium and fine grids. Chien's k-ε turbulence model in full scale.

	K_T	K_Q	η
coarse	100.88	101.30	99.59
medium	100.14	100.36	99.78
fine	100.00	100.00	100.00

Table V. Performance coefficients expressed as percentages of the fine grid solutions for the coarse, medium and fine grids. Chien's k-ε turbulence model in model scale.

	Kt	Kq	Eta
coarse	100.53	102.68	97.908
medium	99.77	100.87	98.905
fine	100	100	100

6. VALIDATION AT MODEL SCALE

In this section, validation data for the design condition of an earlier version of the reference propeller are presented. Figure 8 illustrates results from paint tests showing portions of laminar and turbulent flow on smooth and LE roughened surfaces. Figure 9 shows the corresponding numerical results obtained using the SST k-ω and the Chien's k-ε turbulence models. The former computation is made with fully turbulent flow and the streamlines are similar to the roughened surface streamlines in the tests, except for the laminar patch at the root on the pressure side. The latter computation was made trying to reproduce qualitatively a flow pattern similar to that in the paint tests with smooth surfaces, enforcing low background turbulence. In this way, an indication of change in performance coefficients with growing extent of laminar flow is obtained.
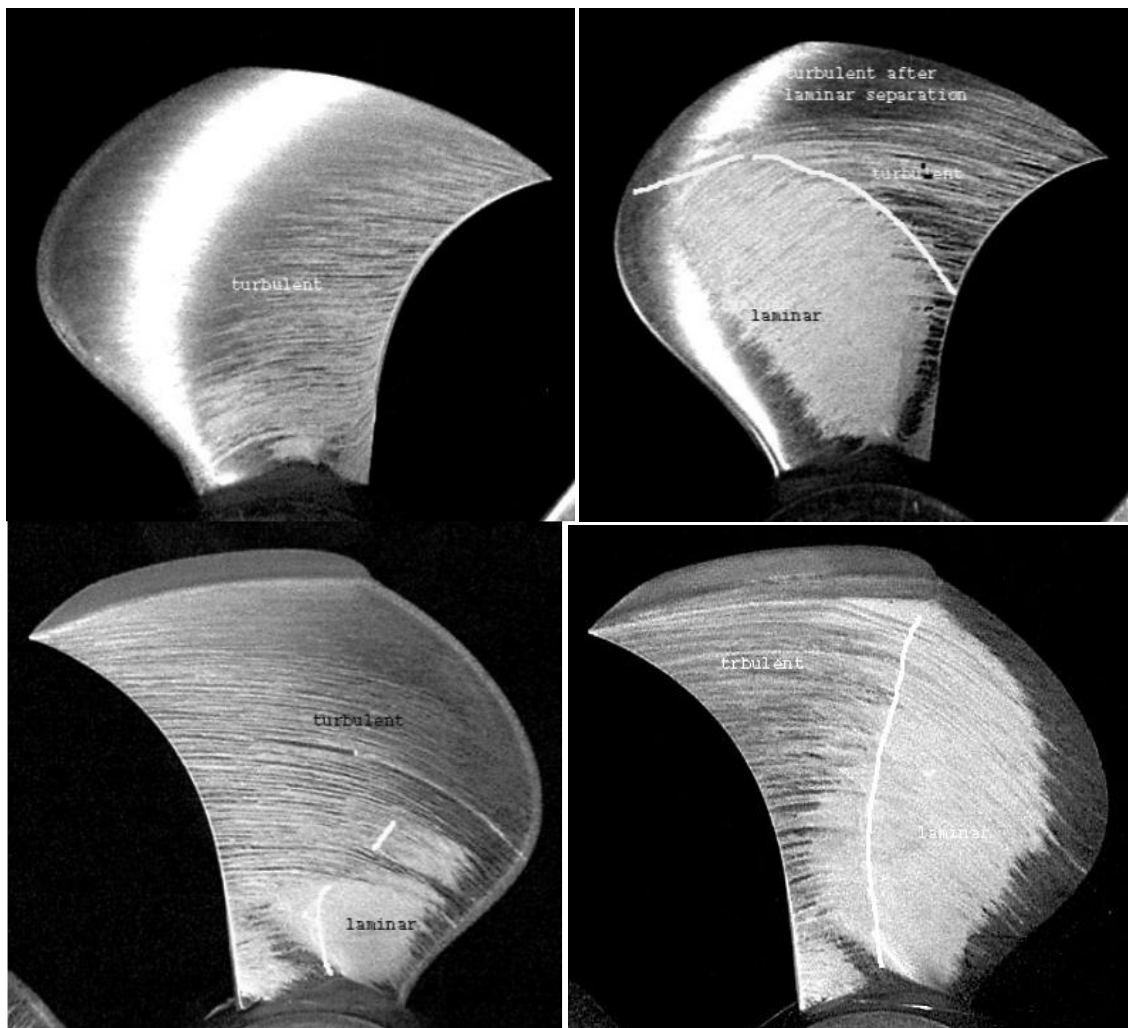

Figure 8. Model test streamlines from paint tests on the suction (up) and pressure (down) sides of the blade for an earlier version of the reference geometry under design condition. Rough (left) and smooth (right) surfaces.
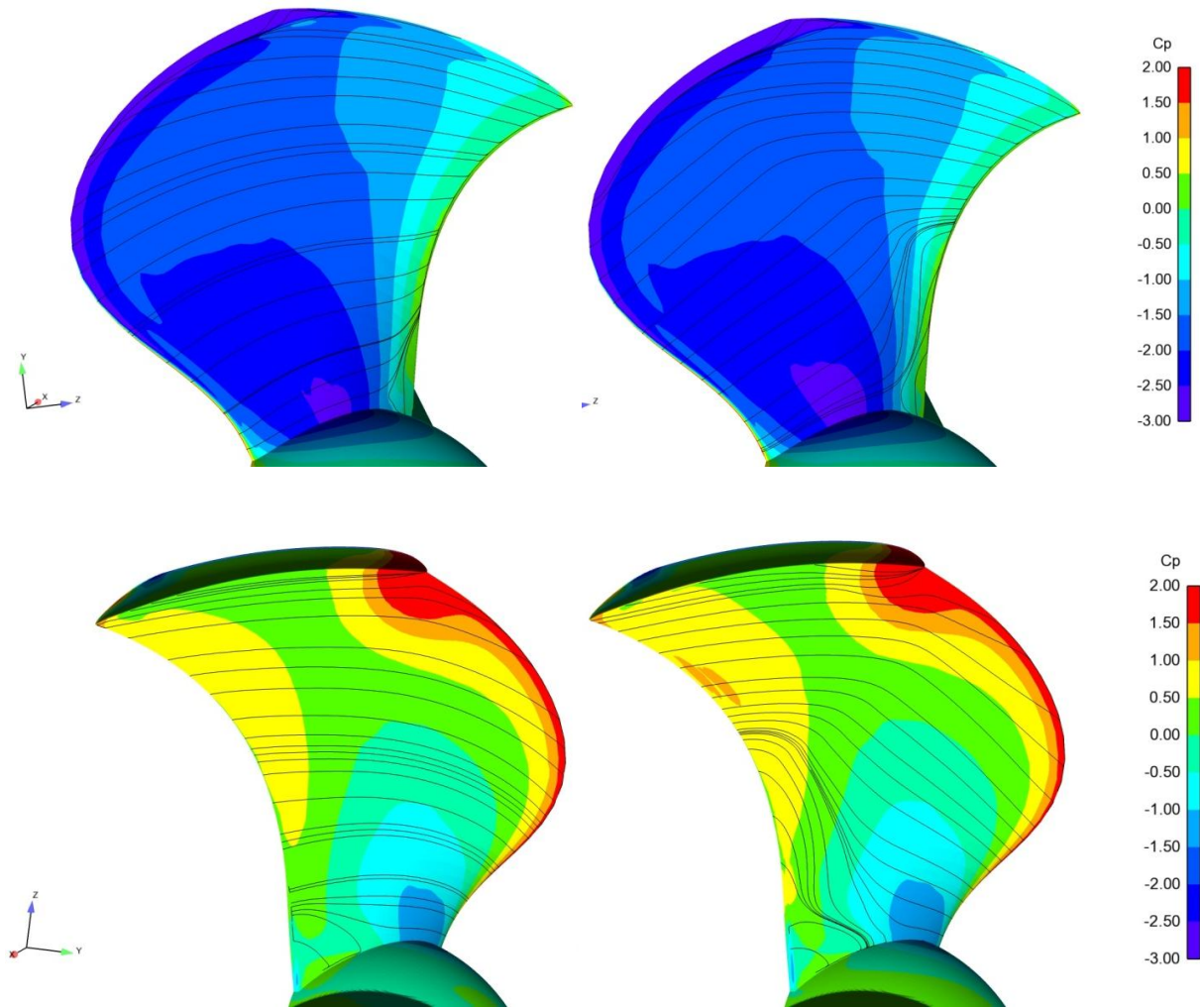
Figure 9.Streamlines from numerical simulation on the suction (up) and pressure (down) sides of the blade for an earlier version of the reference geometry under design condition. Fully turbulent, SST k-ω (left) and partially laminar, Chien's k-ε (right) flow. The k-ε computation was made with low background turbulence to obtain a pattern similar to that in paint tests with smooth surfaces.

The k-ε computations present laminar flow detachment at the lower radii. Figure 10 compares numerical performance coefficients to model tests results. The thrust and torque coefficients are well predicted in the computations as well as the efficiency for Chien's k-ε model. The efficiency prediction for the SST k-ω model is somewhat underpredicted. The efficiency is larger with the k-ε model due to the lower skin friction connected to laminar flow.

The geometry variation study in the next section will be made with the SST k-ω model, assuming at model scale also fully turbulent flow in the comparisons of tip loaded propellers with different plate shapes.

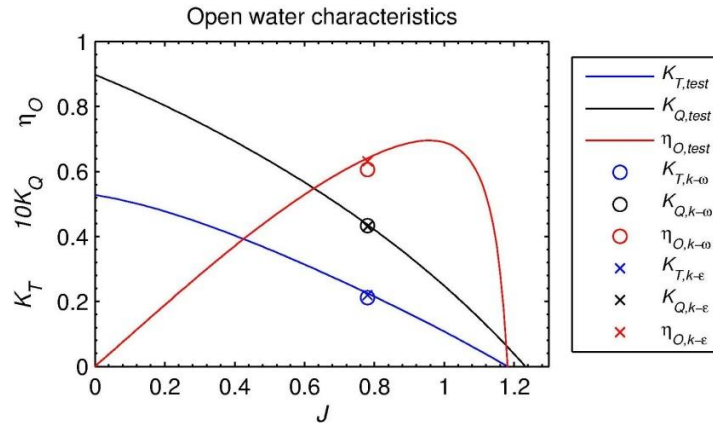Figure 10. Comparison of performance coefficients at model scale. Model tests versus numerical results obtained with the SST k-ω and Chien's k-ε turbulence models.

7. ANALYSIS OF RESULTS

The input data used for the numerical analysis are presented in section 3.

7.1 Influence of Grid Size on Performance Prediction

In general, computations with the coarse meshes showed same trends in performance prediction than those with the fine ones, which indicates that even the coarse grids captured the main features of the flow affecting global forces. For example, Figures 11, 12 and 13 show the influence of the grid size on the efficiency prediction for the geometry variations subject to study. They illustrate the cases of Chien's k-ε turbulence model in full scale, SST k-ω turbulence model in full scale and SST k-ω turbulence model in model scale, respectively. The light bars represent computations on the coarse grid, and the dark bars, computations on the fine grid. Each number in the abscissa represents a variation of endplate shape (see Table I). It is apparent that the trends are identical, even though the absolute level of efficiency changes in about less than 0.5 percent from the coarse to the fine grids for the k-ε model in full scale. For the k-ω model in full and model scale, the differences are even smaller.

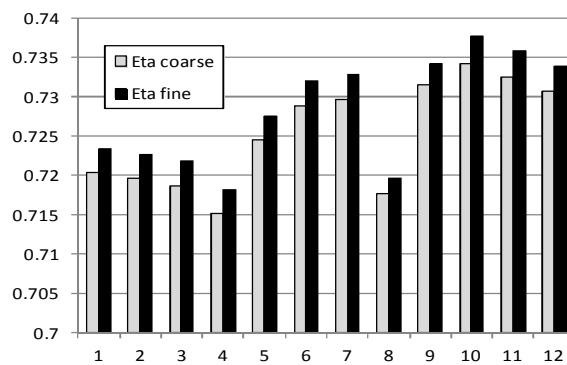Similar behavior was found in the comparison of thrust (K_T) and (K_Q) coefficients.

Figure 11. Comparison of efficiency predictions for 12 endplate versions using the coarse (white) and fine (black) grids. Chien's k-ε turbulence model in full scale
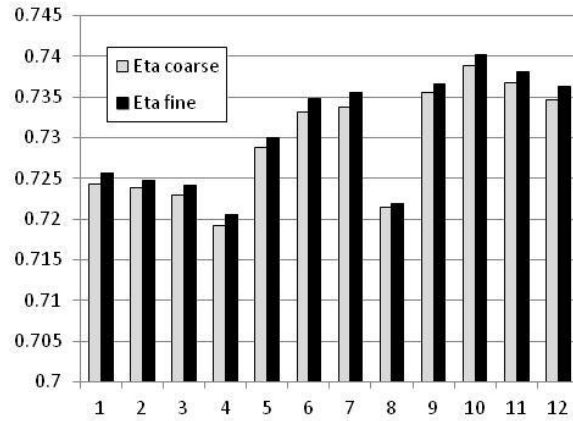
Figure 12. Comparison of efficiency predictions for 12 endplate versions using the coarse (white) and fine (black) grids. SST k-ω turbulence model in full scale
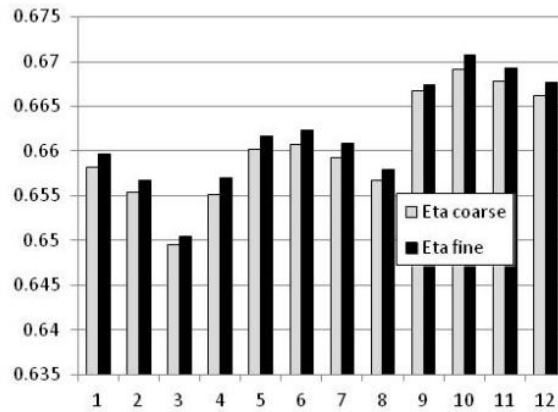

Figure 13. Comparison of efficiency predictions for 12 endplate versions using the coarse (white) and fine (black) grids. The baseline is propeller no. 1. SST k-ω turbulence model in model scale

7.2 Scaling of Reference Geometry

Figure 14a shows the pressure distributions and streamlines predicted at full scale with the SST k-ω, Chien's k-ε and Spalart-Allmaras turbulence models for the input data presented in section 3. There are no qualitative differences among the turbulence models. Figure 14b shows the corresponding figures at model scale. The k-ω and the Spalart-Allmaras turbulence models present a small flow detachment area at the lower radii of the trailing edge mainly on the suction side. For the k-ε model with low background turbulence, the detachment area is much larger and typical streamlines pointing somewhat outwards of laminar flow are apparent.

Table VI shows the effect of scaling on the performance coefficients for the baseline propeller. The percentages represent full-scale values relative to model-scale ones. In the case of the SST k-ω and Spalart-Allmaras turbulence models, the flow is turbulent at both model and full scale and the predicted scale effect of efficiency for the lightly unloaded condition is large. The scale effect on thrust and efficiency is about 1 percent lower for the Spalart-Allmaras model. For the k-ε turbulence model, the flow is partially laminar at model scale and the related lower friction makes the scale effect on efficiency smaller.
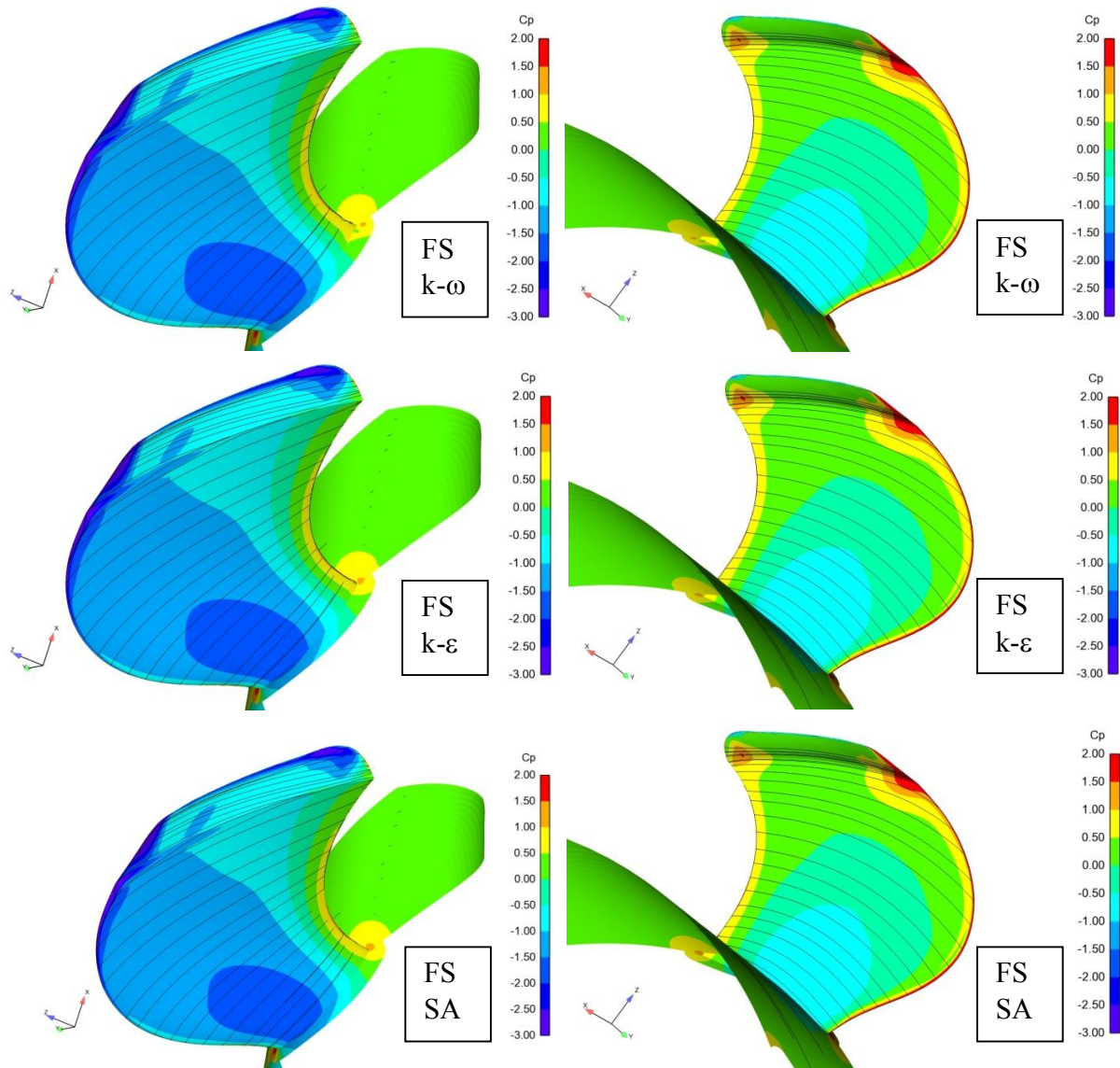
Figure 14a. Comparison of full-scale pressure distributions and streamlines on the suction (right) and pressure (left) sides of the blade for the reference geometry with SST k-ω, Chien's k-ε and Spalart-Allmaras (SA) turbulence models. FS=full scale.

Table VI. Scale Effect on performance coefficients with SST k-ω, Chien's k-ε and Spalart-Allmaras (SA) turbulence models

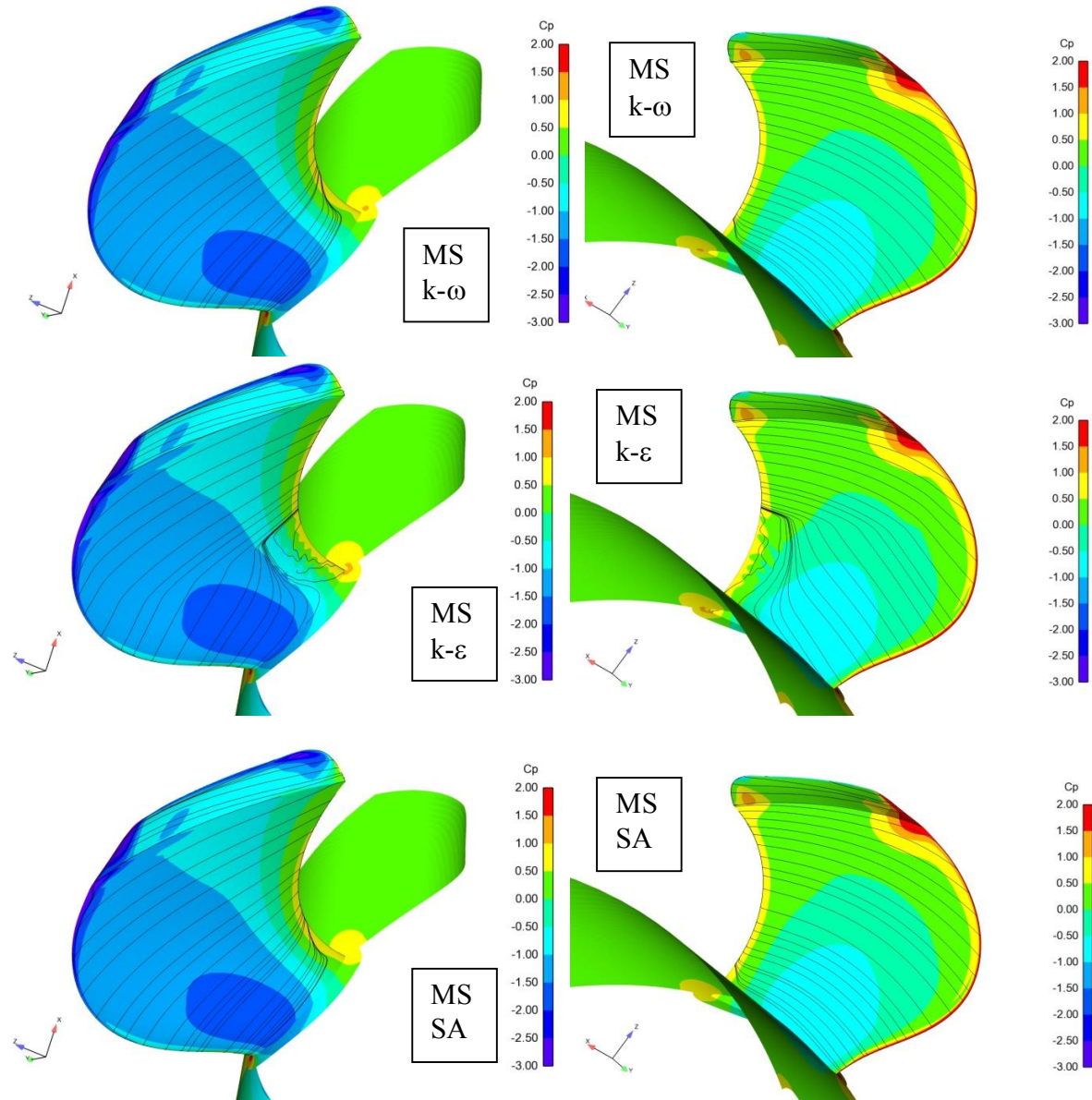| Scale effect	ΔK_T(%)	ΔK_Q(%)	$\Delta \eta$(%)
k-ω	6.3	-3.4	10.0
k-ε	2.1	-3.0	5.4
SA	4.9	-3.7	8.9

Figure 14b. Comparison of model scale pressure distributions and streamlines on the suction (right) and pressure (left) sides of the blade for the reference geometry with SST k-ω, Chien's k-ε and Spalart-Allmaras (SA) turbulence models. MS= model scale.

Figure 15 illustrates the variation of scaling with the loading coefficient, $C_T = 8K_T/(\pi J^2)$, where K_T is the thrust coefficient and J the advance number. The SST k-ω turbulence model was used. In general, the absolute percentages of scaling on efficiency, thrust and torque are larger for low propeller loadings, being the scaling on torque negative. At the design condition, the scaling on efficiency is around 7-8 percent, corresponding to the inner points in the curves of the figure.
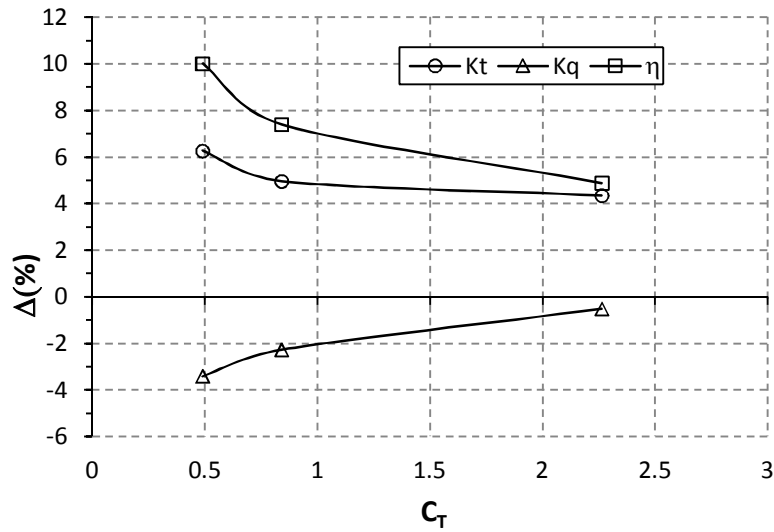
Figure 15. Influence of propeller loading on scaling in percentages relative to model scale values. SST k-ω turbulence model.

7.3 Influence of Geometry on Performance Scaling

The quality of the geometry variations can be assessed by the relative changes in efficiency. The predictions of efficiencies at full scale for the SST k-ω turbulence model are similar to those for Chien's k-ε model.. This is illustrated in Figure 16, which combines the fine grid efficiencies of Figs. 11 and 12.

At model scale, the absolute values of efficiency are smaller than at full scale for the SST k-ω model as expected. The relative performance predictions at model scale somewhat differ from full scale. This is illustrated in Figure 17, which combines the fine grid efficiencies of Figs. 12 and 13. The differences are visible for geometries 1-3 corresponding to changes in flap angle and for geometries 4-7 corresponding to changes in plate contraction. The former one presents larger variations in efficiency at model scale than at full scale even though the ranking of the geometries from the standpoint of efficiency would be the same (the best geometry is number 1). The latter one presents a different ranking: at model scale, the best geometry is number 6 and at full scale, number 7. For geometries 8-9 (sweep), variations in efficiency are somewhat larger at full than at model scale. For geometries 10-12, the relative changes in model and full scale are similar.
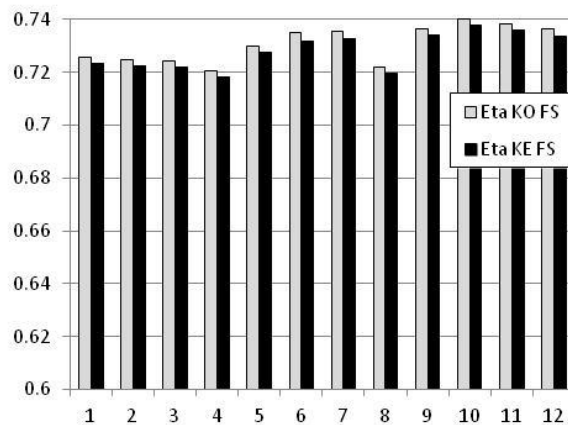

Figure 16. Comparison of efficiency predictions for 12 endplate versions at full scale using the SST k-ω (white) and Chien's low Reynolds number k-ε (black) turbulence model. The baseline is propeller no. 1.
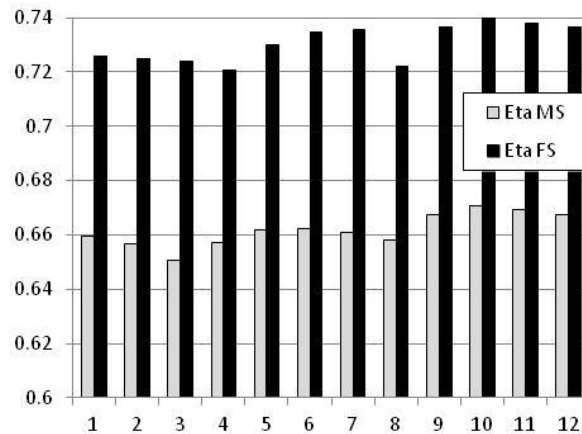
Figure 17. Comparison of efficiency predictions for 12 endplate versions using the SST k-ω turbulence model. Model (white) and full (black) scales. The baseline is propeller no. 1.
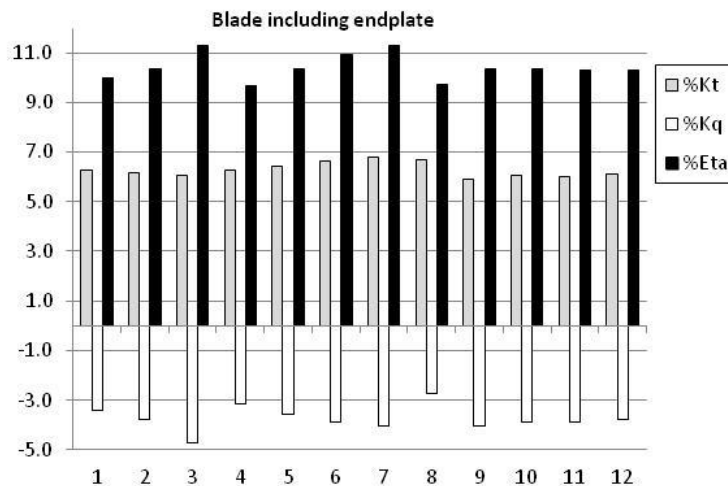

Figure 18. Scale effect on performance coefficients for 12 CLT propellers with different endplates using the SST k-ω turbulence model. Full scale relative to model scale values in percentages. The baseline is propeller no. 1.

Figure 18 shows the scale effect on performance coefficients for the different geometries. The scaling on thrust is around 6 percent increase (slightly above) in average. The scaling on torque is around minus 3-4 percent. The scaling on efficiency is around 10 percent increase (slightly above) in average. Figure 19 shows the scale effect which results from excluding the forces on the endplate. It is apparent that the scaling on thrust is slightly below 6 percent and the scaling on torque is about minus 2 percent on average. The efficiency improvement is around 8 percent. In other words, the effect of the endplate increases the scaling on efficiency in 2 percent, being the main reason the reduction of torque.

Figure 20 illustrates the effect of scaling on the pressure and frictional component of the endplate axial drag. The drag is non-dimensionalized in the same way as the thrust coefficient, i.e. using the density, the square of the rps and the diameter to the fourth power. The full-scale frictional component is reduced to about 47 percent of its model-scale magnitude. The full-scale pressure component changes in +/- 4 percent of its model scale value depending on the type of endplate modification: only the low plate contraction cases (no. 6 and 7) and the plate cutting cases (no. 10, 11 and 12) result in pressure drag decrease. Figure 21 presents the total drag in terms of minus K_T.
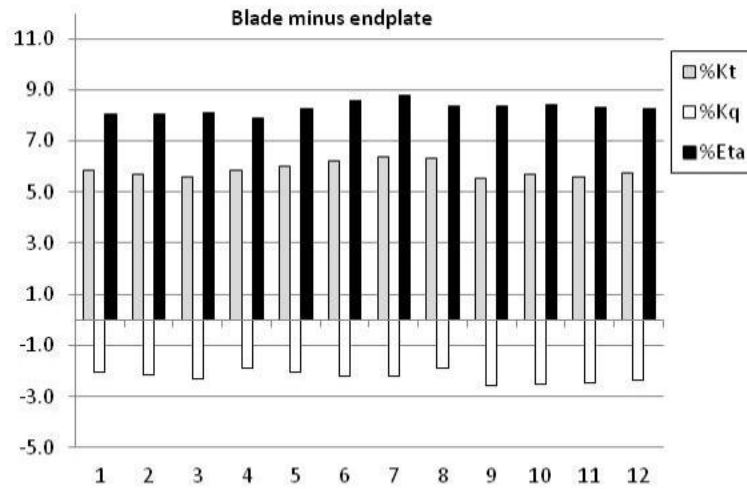
Figure 19. Scale effect in percentages on performance coefficients for 12 CLT propellers with different endplates using the SST k-ω turbulence model. Forces on the endplate are not considered. The baseline is propeller no. 1.

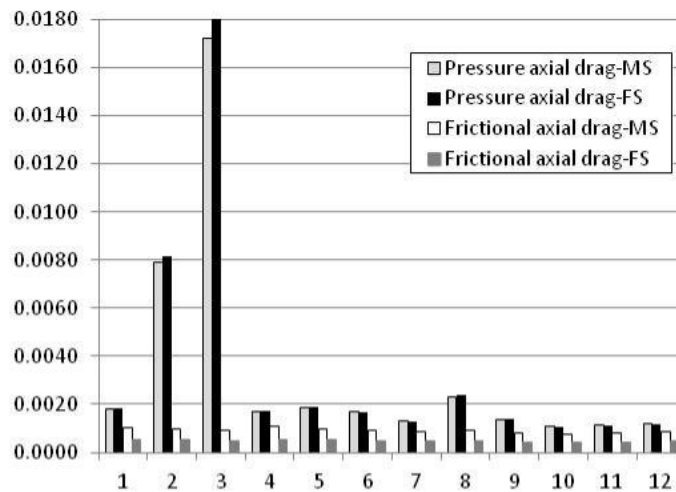*Figure 20. Model versus full scale frictional and pressure components of endplate axial drag for 12 shape variations using the SST k-ω turbulence model. Forces are expressed in terms of minus K_T. The baseline is propeller no. 1.*

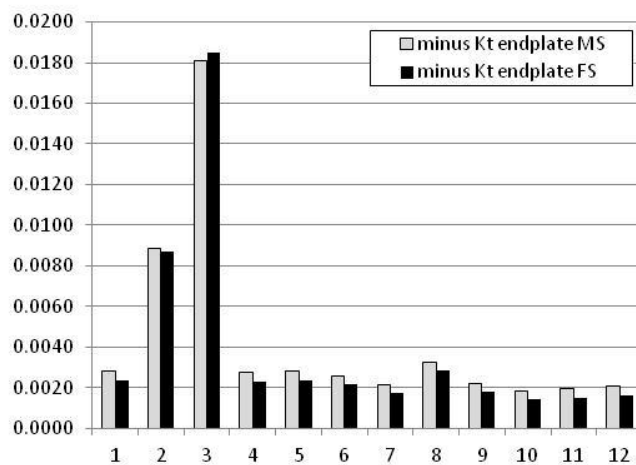*Figure 21. Scale effect on endplate axial drag for 12 shape variations using the SST k-ω turbulence model. Drag is expressed in terms of minus K_T. The baseline is propeller no. 1.*
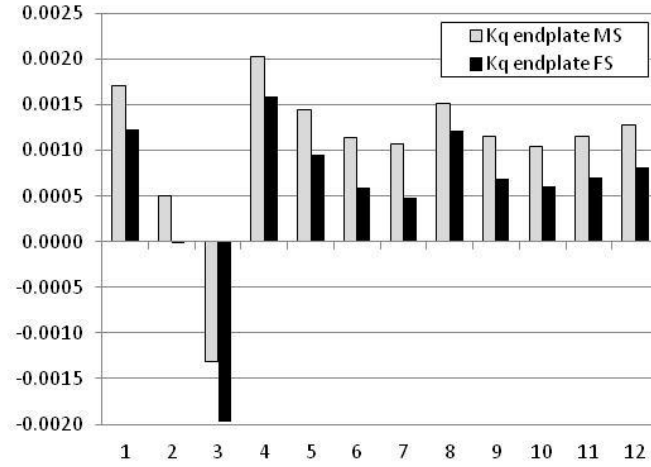
Figure 22. Scale effect on endplate torque for 12 shape variations using the SST k-ω turbulence model. The baseline is propeller no. 1.

Figure 22 illustrates the effect of scaling on the torque component of the endplate. The full-scale torque is reduced in about ΔK_Q=0.0003-0.0006 for the different geometries. It is interesting to note that in full scale the 10 deg flap angle modification (case no. 2) does not produce increment of torque, contrary to model scale. As noted in Sánchez-Caja et al. (2014), flap angle modifications result in negative (backward) endplate thrust due to the orientation of the plate. The torque also decreases since the projection of the total endplate force on the circumferential direction is opposite to the relative inflow direction due to the plate inclination.

7.4 Circulation Scaling

In Sánchez-Caja et al. (2014) the influence of the endplate shape on the radial distribution of circulation was analyzed at full scale using the Chien's k-ε model. The shape and orientation of the endplate had a clear influence on the radial distribution of circulation at the tip. Here, we focus on the influence of scaling on the radial distribution of circulation: model scale and full scale geometries are analyzed using the SST k-ω model.

The magnitude of the bound circulation is derived from the field of induced tangential velocities behind the propeller as follows,

$$\Gamma(r) = \frac{2\pi r U_T}{Z} \qquad (2)$$

where U_T is the average induced tangential velocity at radius r behind the propeller and Z is the number of blades. In the RANS computations, the radial loading can be calculated at the very trailing edge of the blade (or very close to it) contrary to model test measurements. In this way, the radial location of circulation is not affected by flow contraction behind the propeller.

In fact, the circulation as defined in equation (2) can be calculated in two different ways. In the first way, U_T is calculated as the averaged tangential velocity over the circular arc connecting the trailing edges. The second way is the same but excluding the wake region just behind the trailing edge of the blade, i.e. the velocity is averaged only in the "potential-flow" region of the arc. The former way yields a *total* circulation that includes both a "potential-flow" component and a "viscous-flow" component. The second one includes only the "potential-flow" component.

If we intend to compare RANS-based circulations with those obtained using potential flow theory (for example, lifting line), we should use the second way of calculation. With this approach, we are able to assess to what extent target distributions of circulation in a propeller design are actually accomplished.

Figures 23-26 illustrate the impact of scaling on the radial distributions of circulation for the cases of the baseline propeller, the propeller with minimum contraction, that with maximum plate cutting, and that with 30 deg flap angle, respectively. The circulation is made non-dimensional with $2\pi RV$, being R the propeller radius and V the inflow velocity. Both the total and the potential-flow (PF) distributions of circulation are presented at model (MS) and full (FS) scale.

In general, the *total* circulation curves are very similar at the inner radial stations, independently of the scale. In contrast, at the outer radial stations, they are higher at model scale than at full scale, with   positive slopes of circulation larger at model scale. Viscous drag affecting the velocity field in the wake of the blades is the main responsible for the differences in total circulation.

The *potential flow* circulation curves at model scale are lower than at full scale over most of the span with larger average slopes. Larger slopes in *potential-flow* circulation distributions are indicative of larger induced drag. Consequently, the propeller induced drag at model scale is somewhat larger than that at full scale in all cases.

These observations are in line with the findings in Sánchez-Caja et al. (2014) that propellers number 7 (Fig. 24) and number 10 (Fig. 25) have better efficiency at full scale than propellers number 1 (Fig. 23) and number 3 (Fig. 26), being the smaller drag of the former ones (smaller circulation slopes) the reason for better efficiency. The figures present some disturbances in the circulation at the propeller tip because some points used for the evaluation of circulation fall inside the wake behind the endplates. The blade geometry remained untouched in the different propeller versions.

Note that contrary to the potential flow circulation curves, the total circulation curves cannot be directly related to the amount of thrust developed by the propeller. This is due to the spurious viscous component of circulation present in the total circulation.
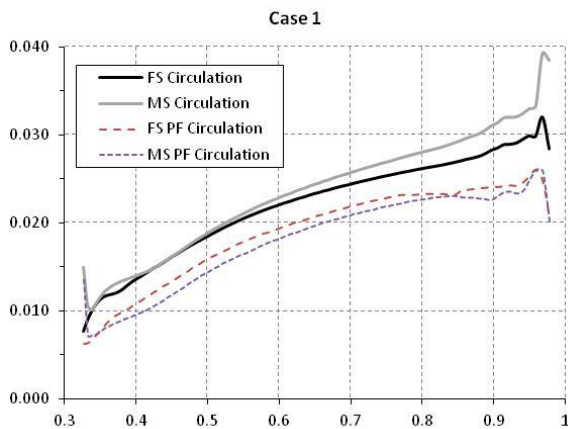

Figure 23. Radial distribution of bound circulation for the baseline propeller (1).
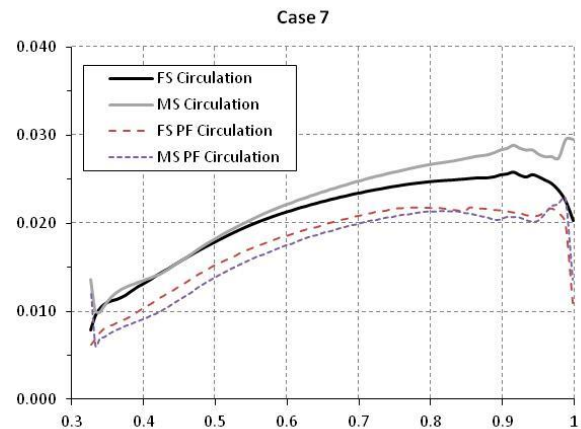

Figure 24. Radial distribution of bound circulation for the propeller with lowest contraction (7)
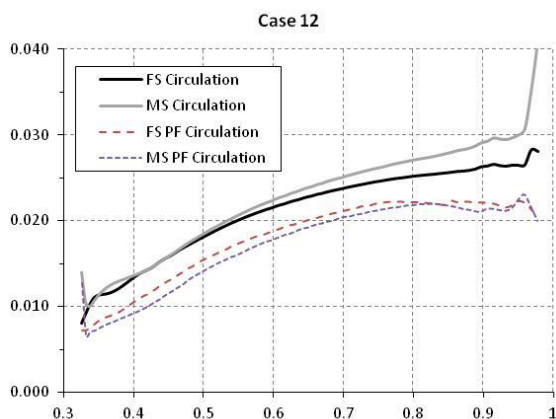

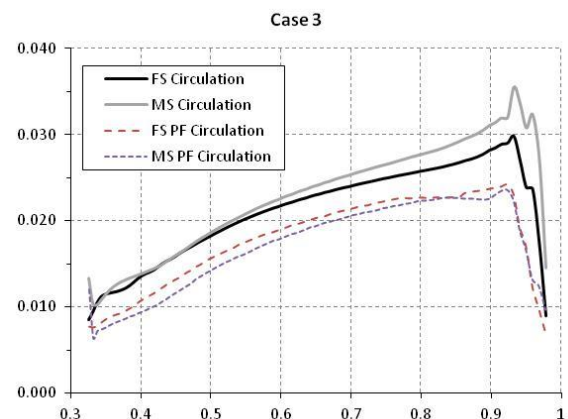*Figure 25. Radial distribution of bound circulation for the propeller with largest cutting (12).*

Figure 26. Radial distribution of bound circulation for the propeller with largest flap angle (3).

8. DISCUSSION

Several variations of endplate geometry have been tested from the standpoint of scaling using code FINFLO with the pressure correction method. The study has been made mainly with the SST k-ω turbulence model, even though some computations were made also with Chien's k-ε turbulence model like the analysis of all full scale cases and of the model scale case for the baseline geometry, and with the Spalart-Allmaras turbulence model for the baseline geometry. The Reynolds number at model scale is 10^6 and at full scale $5*10^7$. The computations with the SST k-ω model were all fully turbulent and presented very limited turbulent separation at the trailing edge close to the hub at model scale. Computations with Chien's k-ε model at model scale were made with low background turbulence in order to have an understanding of trends in scaling effects with partial laminar flow. The computations presented at the lower radii portions of laminar flow with streamlines pointing somewhat outward from the axis followed by flow detachment. Due to the lower frictional drag connected to laminar flow, the model scale performance is closer to the full scale one provided that flow separation is not extensive. Extensive flow separation at model scale would result in deterioration of performance, visible as a reduction of thrust and torque coefficients. At full scale, both turbulent models yield similar results.

Even though the ranking of the various geometries from the standpoint of efficiency is similar for most of the alternative endplate shapes when using either model- or full-scale results, different trends are found in some cases. In particular, for plate contraction, model scale results rank geometry number 6 as the best one whereas full-scale results rank number 7. For sweep and flap angle variations, the relative increments in efficiency also vary from model to full scale. For plate cutting, relative increments in efficiency are similar.

For the moderately unloaded off design condition, the SST k-ω turbulence model predicts a scaling of about 6 percent on thrust and of about minus 4 percent on torque, which amounts to a 10 percent in efficiency. The Spalart-Allmaras model yields similar results although the scaling in thrust was 1 percent less, which resulted in 9 percent scaling on efficiency. The k-ε model with partial laminar flow predicts a scale effect of 5 percent in efficiency. The scaling on efficiency is strongly dependent on the type of flow regime at model scale.

When forces on the blade alone without endplate are considered, the scale effect on efficiency with the SST k-ω model drops from 10 to 8 percent. The scaling of drag on the endplate is responsible for the difference. Comparing to ordinary propellers, the CLT propeller scaling on efficiency is expected to be further larger than that 2 percent (10 minus 8) for this particular working point. This is because conventional propellers are less loaded at the tip, which would make most probably their own scaling effect under similar working conditions lower than 8 percent.

The scaling on the frictional component of axial drag is similar for the various endplates, around 45-49 percent reduction. On the other hand, the pressure component of drag changes in +/- 4 percent of its model scale value depending on the type of endplate modification. The latter is usually larger in absolute value than the former, and therefore, it is the main contributor to changes in efficiency among the different endplates. In other words, pressure forces on the endplate should be controlled in the shape optimization process.

The effect of scaling on the radial distribution of circulation over the blade span is illustrated for some endplates. In general, all the curves present larger positive slopes of circulation at model scale than at full scale. Consequently, the propeller viscous and induced drag components at model scale are larger than at full scale.

9. CONCLUSIONS

The incompressible viscous flow around CLT propellers with different types of endplates has been simulated by solving the RANS equations with various turbulence models using the pressure correction method. The FINFLO code was used for the calculations. A grid study was made using 3 grids with ratios 1, 1.41 and 2 for the computations made at model and full scales. The finest grids contained about 2.4 million cells. Trends in performance coefficients scaling were shown for several types of shape variations. Important features of the flow affecting scaling were identified on a basis of pressure distributions and overall forces on the blades and endplates. The study reveals also how the radial distribution of circulation is affected by scaling.

The differences between the computational results obtained using either fully turbulent or partially laminar flow at model scale and their corresponding scaling are indicative of the importance of taking into account the right type of flow regime in model test extrapolation procedures.

A way of extracting the "potential flow" component of the radial distribution of circulation is presented, which allows assessing to what extent target distributions of circulation in a propeller design are actually accomplished in a viscous flow context (RANS).

Differences found between model and full scales in ranking alternative designs make model scale analysis questionable for some type of modifications when full-scale performance is sought.

REFERENCES

Abdel-Maksoud, M., & Heinke, H.-J., 2002. 'Scale effects on ducted propellers', Proceedings of the 24th ONR Symposium on Naval Hydrodynamics, Fukuoka, Japan, July 2002.

Cheng. H-J, Chien, Y-C, Hsin, C-Y., Chang K., Chen, P., 2010. "A numerical comparison of end-plate effect propellers and conventional propellers", Journal of Hydrodynamics, 22(5), supplement :495-500.

Bertetta, D., Brizzolara, S.,Canepa, E., Gaggero, S., and Viviani, M., 2012. "EFD and CFD Characterization of a CLT Propeller", International Journal of Rotating Machinery Vol. 2012, Article ID 348939, 22 pages.

Chicherin, I.A., Lobatchev, M.P., Pustoshny, A.V. and Sanchez-Caja, A., 2004. On a Propulsion Prediction Procedure for Ships with Podded Propulsors Using RANS-Code Analysis. The 1st International Conference on Technological Advances in Podded Propulsion April 14-16, 2004, University of Newcastle (U.K.)

Gaggero, S., Brizzolara, S., 2011. "Endplate Effect Propellers: a Numerical Overview", IMAM'2011 XIV Congress of the International Maritime Association of the Mediterranean, Genova, Italy, October, 2011.

Funeno, I., 2002. "On Viscous Flow around Marine Propellers – Hub Vortex and Scale Effect –", Journal of Kansai Society of Naval Architects, No. 238, pp. 17–27.

Haimov, H., Vicario, J., Del Corral, J., 2011. "RANSE Code Applicaton for Ducted and Endplate Propellers in Open Water", Second International Symposium on Marine Propulsors SMP'11, Hamburg, Germany, June 2011.

Hsin, C.-Y., Chang, K.-K., Chi, R.-C., and Chen, P.-F., 2010. "Design and Analysis of the End Plate Effect Propellers," Proc. of 28th Symposium on Naval Hydrodynamics, Pasadena, CA USA, 12-17 Sept 2010.

Kawamura, T. and Omori, T., 2009. "Reynolds number effect on propeller performance in open water," Journal of the Japan Society of Naval Architects and Ocean Engineers, Vol.10, pp.29-36.

Krasilnikov, V., Sun, J., and Halse, K. H.,2009. "CFD investigation in scale effect on propellers with different magnitude of skew in turbulent flow", Proc., First Intl. Symp. on Marine Propulsors (SMP'09), Trondheim, Norway.

Krasilnikov, V.I., Sun, J., Zhang, Zh., & Hong, F., 2007. 'Mesh generation technique for the analysis of ducted propellers using a commercial RANSE solver and its application to scale effect study', Proceedings of the 10th Numerical Towing Tank Symposium (NuTTS'07), Hamburg, Germany, September 2007.

Koushan, K. & Krasilnikov, V.I., 2008. 'Experimental and numerical investigation of open thrusters in oblique flow conditions', Proceedings of the 27th ONR Symposium on Naval Hydrodynamics, Seoul, Korea, October 2008.

Li, D.-Q., Berchiche, N., Janson, C.-E., 2006. 'Influence of Turbulence Models on the Prediction of Full-Scale Propeller Open Water Characteristics with RANS methods'. 26th Symposium on Naval Hydrodynamics, Rome, Italy.

Lobachev, M.P., Chitcherin, I.A., 2001. "The Full Scale Estimation for Podded Propulsion System by RANS Method." Lavrentiev Lectures, St. Petersburg (Russia), June 19-21.

Mertes, P. and Heinke, H.-J., 2008. "Aspects of the Design Procedure for Propellers Providing Maximum Bollard Pull," ITS 2008, Singapore.

Menter, F. R., Langtry, R., Völker, S., 2006. 'Transition Modelling for General Purpose CFD Codes'. Flow, Turbulence and Combustion, Volume 77, Numbers 1-4, Springer Netherlands.

Müller, S.-B., Abdel-Maksoud, M., and Hilbert, G., 2009. "Scale effects on propellers for large container vessels", Proc., First Intl. Symp. on Marine Propulsors (SMP'09), Trondheim, Norway.

Sanchez-Caja, A., Rautaheimo, P., Salminen, E., Siikonen, T., 1999. "Computation of the Incompressible Viscous Flow around a Tractor Thruster Using a Sliding-Mesh Technique", Proc. of The Seventh International International Conference on Numerical Ship Hydrodynamics.

Sanchez-Caja, A., Ory, E., Salminen, E., Pylkkänen, J. & Siikonen, T., 2003. "Simulation of Incompressible Viscous Flow Around a Tractor Thruster in Model and Full Scale". The 8th International Conference on Numerical Ship Hydrodynamics, Busan (Korea), September 22-25.

Sánchez-Caja, A., Sipilä, T., Pylkkänen, J., 2006. "Simulation of the Incompressible Viscous Flow around an Endplate Propeller Using a RANSE Solver", 26th Symposium on Naval Hydrodynamics Rome, Italy.

Sánchez-Caja A., González-Adalid J., Pérez-Sobrino M. and Saisto I., 2012. "Study of End-Plate Shape Variations for Tip Loaded Propellers Using a RANSE Solver". 29th Symposium on Naval Hydrodynamics Gothenburg, Sweden, 26-31 August 2012.

Sánchez-Caja A., González-Adalid J., Pérez-Sobrino M. and Saisto I., 2014. "Evaluation of End-Plate Impact on Tip Loaded Propeller Performance Using a RANSE Solver". International Shipbuilding Progress, Vol. 61.

Stanier, M., 1998 "The Application of RANS Code to Investigate Propeller Scale Effects", Proc. of 22nd ONR Symposium, Washington, DC, USA, pp. 222-238.

Siikonen, T., Hoffren, J., and Laine, S., 1990. "A Multigrid LU Factorisation Scheme for the Thin-Layer Navier-Stockes Equations", Proceedings of the 17th ICAS Congress, paper 90-6.10.3, Stockholm, Sept. 1990, pp. 2023-2034.

Siikonen, T., 2011. " Developments in Pressure Correction Methods for a Single and Two Phase Flow", Aalto University Report CFD/MECHA-10-2011, pages 63, Espoo, Sept.